JOURNAL OF MATERIALS SCIENCE **38** (2003) 489–497

# *In situ* surface oxidation of Ti-44Al-11Nb alloy at room temperature

P. W. WANG*
*Department of Physics, Bradley University, Peoria, IL 61625, USA*
*E-mail: pwang@bradley.edu*

J. WOO‡, M. AVILA§, J. GARCIA§, A. BRONSON¶, S. K. VARMA‡
‡*Department of Metallurgical and Materials Engineering,* §*Department of Physics,*
¶*Department of Mechanical and Industrial Engineering, University of Texas at El Paso, El Paso TX 79968, USA*

The *in situ* surface oxidation of polycrystalline Ti-44Al-11Nb (compositions are in atomic %) alloy was studied at room temperature in an ultrahigh vacuum (66.6 to 80.0 nPa). The native oxide of Ti-44Al-11Nb was removed by sputtering the surface using 2.8 kV argon ions and then high-purity oxygen was carefully dosed onto the aluminide surface. After each oxygen dosing the surface species, metallic states and oxidized states, were detected by X-ray photoelectron spectroscopy (XPS). After analyzing the binding energy shifts and the concentration of oxidized species, aluminum oxidized first, then titanium followed by niobium. A reaction sequence model, incorporating the rate-determining step of a dissociative adsorption of oxygen, shows to be consistent with the initial oxidation rate of the Ti-44Al-11Nb intermetallic. 

## 1. Introduction

Titanium aluminides having lighter density than Ni based superalloys would substitute for conventional Ni-based superalloys [1] and automotive engine parts [2, 3]. However, $\gamma$-TiAl alloys have low oxidation resistance at temperatures greater than 800°C and a low ductility at room temperature, as reported by Smarsly and Singheiser [1]. To improve oxidation resistance and mechanical properties, an extensive research into the TiAl, $Ti_3Al$ and their alloys has been pursued and the reader is referred to the reviews by Huang and Chesnutt [4] and Banerjee [5]. Engine parts are sometimes susceptible to corrosive wear, so our research group investigated the room temperature oxidation of a Ti-44Al-11Nb alloy. Although one would expect that high temperature processing would contribute significantly more oxygen than room temperature exposure, the room temperature brittle behavior caused by pinning of dislocations of oxygen atoms [6] may affect corrosive wear. Dary [7] has reported that oxygen enriched layers and oxide films cause reduced room temperature ductility of Ti-22 at%Al-23 at%Nb and even surface cracks, as a result of heat treatment in air at 760°C. In addition, corrosive wear occurring at room temperature may remove the protective scale during abrasive wear conditions, although one would expect that the room temperature oxidation of the surface would become important, if sufficient oxygen is introduced into either the oxide enriched layers or even the lattice. The objective of the present study was to determine the room temperature oxidation of a Ti-44Al-11Nb alloy by using Auger electron spectroscopy (AES) and by X-ray photoelectron spectroscopy (XPS).

Niobium is added as a ternary element to improve the oxidation resistance and mechanical properties at high temperatures [2], although Paul, Appel and Wagner [8] reported that Nb plays no role in strengthening during compression of TiAlNb alloys. Niobium additions to the TiA1 alloy complicate the phase equilibria which must be considered in strengthening and oxidation mechanisms. For example, with an addition of 2 wt% Nb to TiAl, Nb dissolves into the TiA1 and $Ti_3Al$ phases [9] although larger additions may cause the formation of $Ti_{50}Al_{33}Nb_{15}$, or the $\beta$-NbTi phase. Much effort has been made to study the high temperature oxidation of $\gamma$-TiA1 alloys [10–15], with Nb additions having conflicting findings as briefly noted by Roy *et al.* [15]. The role of Nb in oxidation is complicated because it may affect several factors such as: the chemical stability of the $Al_2O_3$ and $TiO_2$ scale [15–17] and the occurrence of $TiNb_2O_7$ [17]; the physical characteristics (e.g., porosity and adherence) of the scale [18]; ternary phase equilibria of Al-Nb-Ti for which Hellwig, Palm and Inden [19] reported the inexistence of ternary phases (i.e., $NbTiAl_3$, $Ti_{45}Al_{35}Nb_{20}$ and $Ti_{45}Al_{45}Nb_{10}$) at 1200°C.

Taylor and Paffett [20] reported on the oxidation of $\gamma$-TiAl from room temperature to 600°C by using XPS and secondary ion mass spectroscopy (SIMS). For the matter here, they found a room temperature oxide having a thickness of 0.3 nm and composed of a mixture of $TiO_2$ and $Al_2O_3$. Shanabarger [21] reported that

*Author to whom all correspondence should be addressed.

the room temperature adsorption kinetics of oxygen on $\alpha_2$-$Ti_3Al$ and $\gamma$-TiAl was independent of Al content and identical to pure Ti for an oxide thickness of 0.45–0.55 nm, as determined by AES. Shanabarger concluded that oxygen dissociated via titanium surface atoms, because the oxygen adsorption was independent of aluminum surface concentration. On a more recent study, Shanabarger [22] reported that the oxygen adsorption does depend on Al content. In the oxidation study of $\gamma$-TiAl by Beye and Gronsky [23] using AES, they found that Ti diffused quickly to the surface after sputtering and Ti diffusion may explain the identical adsorption kinetics of oxygen on $Ti_3Al$ and TiAl. They also reported that the surface oxide on TiAl was $TiO_2$ instead of $Al_2O_3$. In a subsequent investigation, Beye *et al*. [24] focused on a study of the subscale with $\gamma$-TiAl and noted the report of $Al_2O_3$ on the surface at room temperature. Beye *et al*. also characterized the surface oxide as $TiO_2$ at ambient temperatures with an oxide thickness of 200 nm. Geng *et al*. [25] determined by using monochromatic X-ray photoelectron spectroscopy (MXPS), that at room temperature oxidation, the Al/Ti concentration ratio approximates 1.4 for the $Al_2O_3$-$TiO_2$ oxide of a Ti-54Al alloy when exposed to oxygen. The aluminum and titanium content decreases very quickly within the first few seconds of oxygen exposure. From their MXPS study, Geng *et al*. concluded that an $Al_2O_3$ layer develops very quickly at room temperature, although they also suggested the development of $TiO_2$ on the surface, because Ti diffuses through $Al_2O_3$.

The stability of the oxides based on the Gibbs free energy is provided in Table I. Although the Gibbs free energy determines that $Al_2O_3$ is the most stable oxide, the kinetic factors (e.g., oxygen adsorption and diffusion of cations) are obviously not considered. Of course, the multivalency of Ti and Nb would form oxides, which depend on the oxygen potential at the gas/solid interface and along the interdiffusion zone. The oxygen potential for $TiO_{2-x}/Ti_nO_{2n-1}$ coexistence is significantly lower than that available in the AES chamber, so rutile ($TiO_{2-x}$) would obviously form on the surface of the aluminide rather than the Magneli phases ($Ti_nO_{2n-1}$). For a value of $n = 40$, the Gibbs free energy has been calculated from Zador and Alcock's data [26] extrapolated to 300 K. The existence of $Ti^{4+}$ and $Ti^{3+}$ suggested by Taylor and Paffett at room temperature results from the non-stoichiometry of $TiO_{2-x}$ for which Kofstad [28] reported interstitial titanium ions with three and four effective charges.

TABLE I Thermodynamic stability of possible oxides on TiAl

| Reaction | $\Delta G^{\circ}_{f,300\,K}$ (kJ) |
|---|---|
| $2Ti_{40}O_{79} + O_2 = 80TiO_2$ | $-552$[a] |
| $4NbO_2 + O_2 = 2Nb_2O_5$ | $-575$[b] |
| $2NbO + O_2 = 2NbO_2$ | $-694$[b] |
| $2Nb + O_2 = 2NbO$ | $-784$[b] |
| $4/3Al + O_2 = 2/3Al_2O_3$ | $-1054$[b] |

[a]Thermodynamic data extrapolated from experimental data acquired at 1300 and 1400°C [26].
[b]Thermodynamic data taken from Scientific Group Thermodata Europe (SGTE) database [27].

## 2. Experimental

The Ti-44Al-11Nb alloy was made by using Ti, Al and Nb with 99.998 purity levels. Melting was performed in an arc-melter in a deoxidized argon atmosphere to produce buttons. The first melting produced buttons of approximately 10 grams each and repeated melting of the buttons was done to produce a homogeneous distribution of metals. The final rod was cast into a dimension of 10 mm diameter and 80 mm length. After slicing samples to 1 mm thickness, they were metallographically prepared to a 600 grit polish.

Prior to performing Auger electron spectroscopy (AES), each sample was mounted onto a holder and the AES chamber evacuated to 5 to $6 \times 10^{-10}$ Torr (66.6 to 80.0 nPa), similar to the procedure reported by Wang *et al*. [29] for an Al nitride investigation. The sample surface was sputtered by using 2.8 keV argon ions with an ion current of 3.5 $\mu$A, and immediately afterwards, a high purity oxygen gas was leaked through a dosing tube onto the sample surface at room temperature. The sputtering process did not seem to affect the surface content similar to the finding of Beye and Gronsky [23] who reported that the sputtering did not preferentially remove the elements from the surface of $\gamma$-TiAl alloy. The amount of oxygen dosed onto fresh cleaned sample surface was measured by Langmuir (L), which is a product of the vacuum (in Torr) and time (in second) so that one Langmuir equals $10^{-6}$ Torr·sec. After each oxygen dosing X-ray photoelectron spectroscopy was used to detect the oxidation states of the elements on surface.

The primary electron voltage used to generate the Auger electrons was 3.0 kV and the secondary electrons from the surface were collected by a double-pass cylindrical mirror energy analyzer. The kinetic energies of the electrons were plotted as a function of the number of electrons collected. The spectra of the core-level photoelectrons of Al, Ti, and Nb were decomposed and investigated by XPS. The emission of photoelectrons was induced by a 0.834 nm X-ray (Al $K_\alpha$ line) generated by electrons accelerated at 14 keV impacting an aluminum anode at a power level of 225 W. The pass energy of the double-pass cylindrical mirror analyzer was 100 eV.

The XPS spectra was analyzed to determine the oxidation state from the peak position and the concentration of the element from the integrated area formed by the spectra, as well as considering the photoelectron yield from each element. Wagner *et al*. [30] did not report the atomic sensitivity factors for Ti $2p_{1/2}$ and Nb $3d_{3/2}$, so their relative concentrations and their binding energies were determined by using the sensitivity factors of Ti $2p_{3/2}$ and Nb $3d_{5/2}$. However, the peak-to-peak height and Auger sensitivity factor were used instead of the integrated area and the atomic sensitivity factor to calculate the concentration of each element in Auger spectra.

## 3. Results and discussion

The Auger spectra of the Ti-44Al-11Nb alloy sample prior to sputtering showed a large Auger oxygen (KLL) signal at 512 eV and a carbon (KLL) signal at 271 eV, as

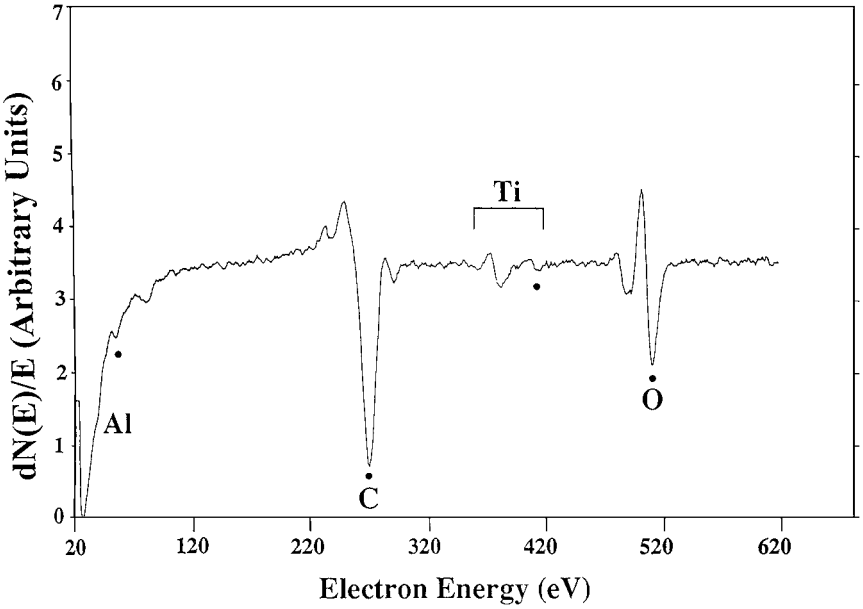


*Figure 1* The AES spectrum of Ti-44Al-11Nb alloy before sputter clean by using 2.8 keV Ar ions. The oxidized Al, Ti and surface contaminants of C and O were observed.

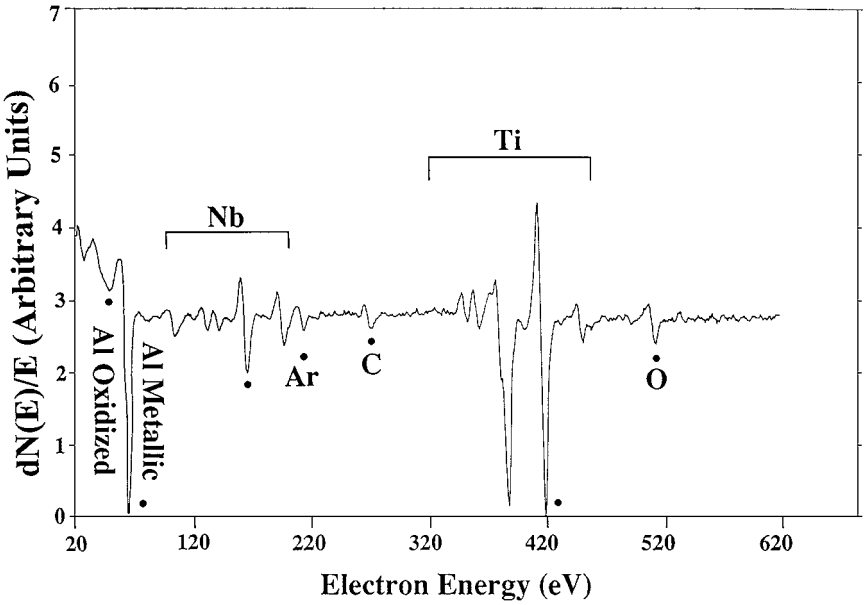


*Figure 2* The Auger spectrum of Ti-44Al-11Nb sample after 105 minutes Ar ion sputtering. The remained C and O on surface were the intrinsic impurities inside the sample. The relative concentrations of the surface species were listed in Table II.

shown in Fig. 1. The Auger signals at 416 eV and 55 eV indicate that very small concentrations of Ti (LMM) and oxidized Al (LMM) resided on the surface. After 105 minutes of sputtering, the AES spectrum revealed that the major Auger signals were Al (oxidized Al at 52 eV and metallic Al at 67 eV), Ti at 418 eV, and Nb at 168 eV (an MNN Auger signal), as shown in Fig. 2. The dot under or beside the differential peak indicates the main Auger signal of that element. However, carbon and oxygen still remained on the surface even after 105 minutes of sputtering. Wang *et al.* [31] also determined that argon sputtering at room temperature would not remove all the oxygen from an Al 6061 surface, because of the reaction between residual oxygen within the UHV chamber and Al, as expected from the $Al_2O_3$ stability. Beye and Gronsky [23] reported the existence of residual oxygen on the surface of $\gamma$-TiAl after argon sputtering. The carbon on the surface may result from the carbon impurity introduced during fabrication. Taylor and Paffett [20] reported in their results of $\gamma$-TiAl (with 2 at% Nb) samples that the impurities of carbon and oxygen were caused by segregants in the grain boundaries of the exposed polycrystalline material. The relative concentrations of Al, Ti, Nb, C and O in atomic percent before and after 2.8 keV argon ion sputtering for 105 minutes have been provided in Table II.

After sputtering for 145 minutes, high purity oxygen was introduced onto the sample surface through a stainless steel tube at dosages of 6, 10, 20, 30, and 40 Langmuir at room temperature. The base pressure of the chamber during the dosing was maintained at $5 \times 10^{-8}$ torr (6.66 $\mu$Pa). After each dosage, the XPS spectra of Al 2p, Nb 3d and Ti 2p were collected. The XPS

TABLE II Concentrations of surface species before and after sputtering

| | Composition (atom %) | | | | | |
|---|---|---|---|---|---|---|
| | Oxidized Al | Metallic Al | Ti | Nb | C | O |
| Before sputtering | 1.5 | Not detected | 1.5 | Not detected | 76.4 | 20.6 |
| After sputtering | 8.4 | 43.2 | 27.8 | 13.0 | 4.4 | 2.8 |

spectra of Al 2p, Ti $2p_{1/2}$ and $2p_{3/2}$, Nb $3d_{3/2}$ and $3d_{5/2}$ before (a) and after 20 L oxygen dosing (b) indicate clearly the oxidation of Al, Ti and Nb species, as shown in Figs 3a and b to 5a and b, respectively. The binding energies (BEs) for Al, Ti and Nb spectra after 20 L exposure shown in Figs 3b, 4b and 5b were corrected for a positive surface charge by substracting 0.22 eV.

Before oxygen dosing, the BE of metallic Al 2p at 72.64 eV nears the value (i.e., 72.65 eV) obtained from pure Al metal [30], and the BE of oxidized Al 2p located at 75.53 eV is 0.83 eV higher than the BE from pure $Al_2O_3$ [30], as shown in Fig. 3a. The increased BE indicates that the electron density surrounding oxidized Al atoms is less than that around Al atoms on an $Al_2O_3$ surface. Niobium atoms have the highest electron negativity in comparison with Al and Ti atoms. Hence, the increased BE of oxidized Al indicates the involvement of Nb atoms in the formation of Al bonding. The surface composition (Table II) indicates only 2.8% oxygen was on the surface and 13% Nb after sputtering. Consequently, electron density around oxidized Al atoms shifts towards Nb and oxygen atoms. Another reason for this higher BE of oxidized Al before dosing is the existence of oxidized Al with oxidation states higher than 3+ (e.g., $AlO_2$ and $AlO_3$), similar to $GeO_2$ [32].

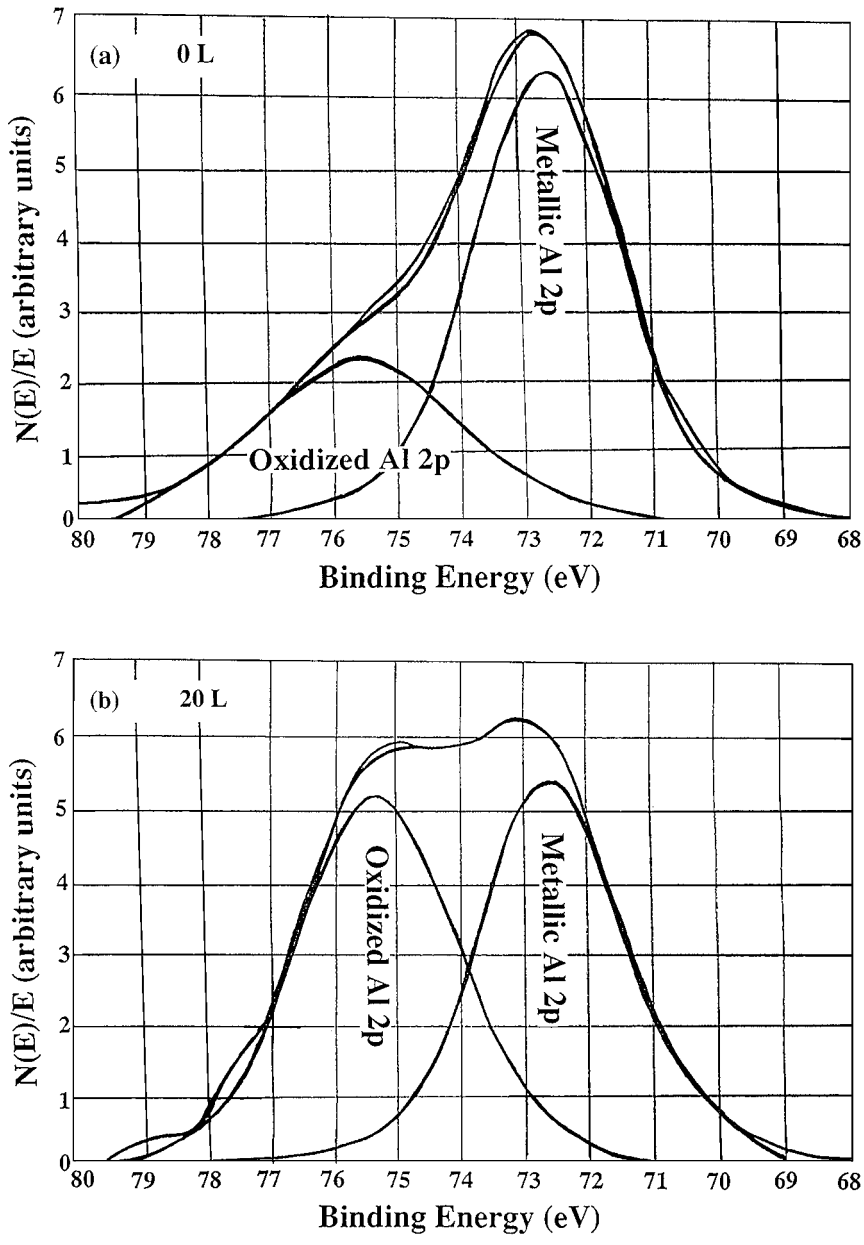


*Figure 3* The XPS spectra of Al 2p, before oxygen dosing (a) and after 20 L oxygen dosing (b). Spectra were decomposed into oxidized state and metallic state by using a fitting program.

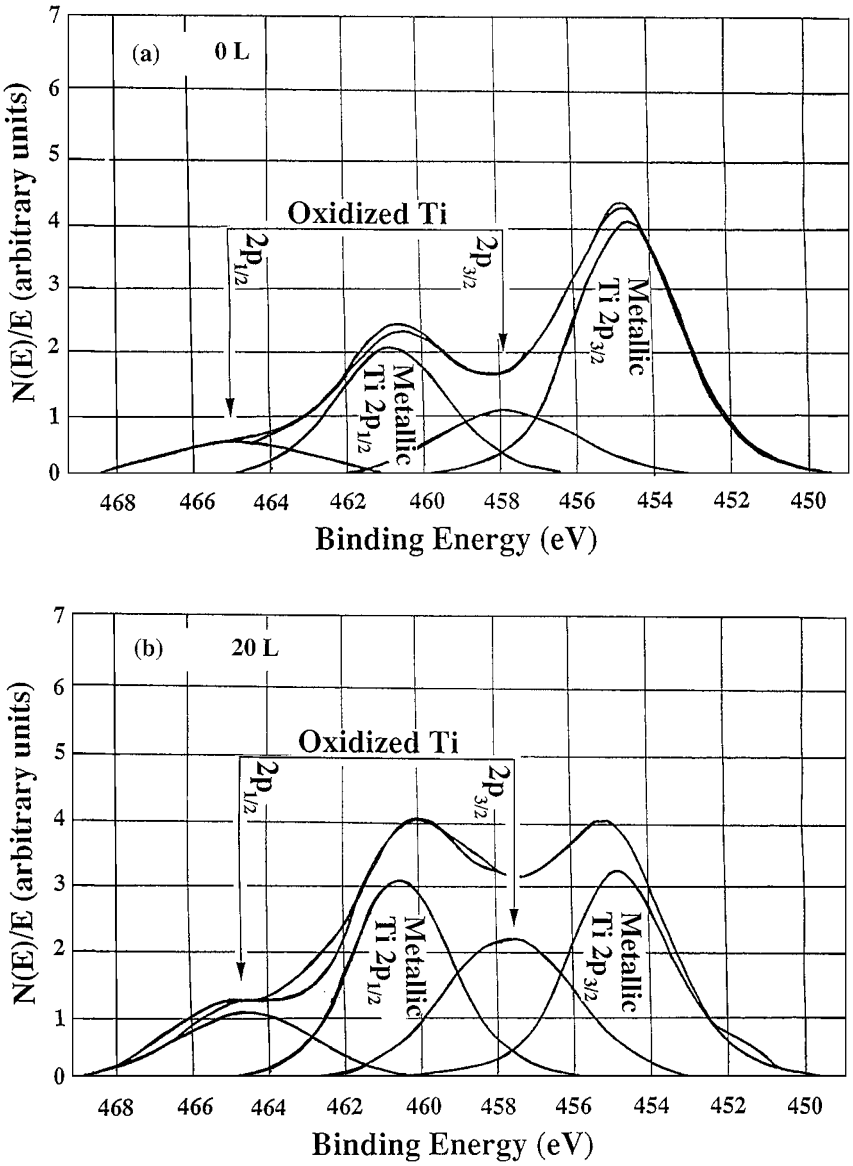


*Figure 4* The XPS spectra of Ti 2p1/2 and 2p3/2 before oxygen dosing (a) and after 20 L oxygen dosing (b). Spectra were decomposed into oxidized state and metallic state by using a fitting program.

The BE of oxidized Al 2p (75.28 eV) after 20 L dosing (Fig. 3b) is higher than the BE (74.70 eV) of oxidized Al 2p obtained from pure $Al_2O_3$ [30]. This implies double or triple oxygen bonding to one Al atom. In comparing the BE of oxidized Al 2p before and after dosing, the BE decreased by 0.25 eV. The shift of the BE to lower values during oxygen dosing clearly shows that oxidation states lower than 3+ may develop and indicates that oxygen bonding with Al may involve single bonding. The BE of metallic Al 2p after 20 L dosing remains the same as before. In fact, Arranz and Palacio [33], Zhukov *et al*. [34], and Zhukov, Popova and Yates [35] have also reported that Al atoms during Al oxidation form one, two and three covalent Al-O bonds.

The BE of metallic Ti $2p_{3/2}$ (454.70 eV) is greater than the BE of metallic Ti metal (453.80 eV) [30], which indicates that the electron density around metallic Ti atoms on the Ti-44Al-11Nb surface is less than that of pure Ti metal. Oxygen increased the BE of Al, which has a higher electron affinity than Ti. With Ti atoms surrounded by Al atoms, the electrons around Ti metal atoms may shift away from their nuclei causing the increased BE of the metallic Ti $2p_{3/2}$. The BE of oxidized Ti $2p_{3/2}$ (457.80 eV) is 0.7 eV lower than the BE of oxidized Ti $2p_{3/2}$ from $TiO_2$ (458.50 eV), as reported by Wagner [30]. The observed lower BE of oxidized Ti was quite unexpected, because only a small amount of oxygen resided on the surface after sputtering although the surrounding Al and Nb atoms do have higher electron affinities. The shift to lower BE on Ti-44Al-11Nb may result from the existence of lower oxidation states than 4+ (i.e., $Ti^{3+}$ or $Ti^{2+}$), which has been reported by Taylor and Paffett [20] and Lu, Bernasek and Schwartz [36]. Lu et al. also reported that $Ti^{2+}$ and metallic Ti atoms were found near the metal-oxide interface after depth profiling.

Similar to the Al 2p, the metallic Ti $2p_{3/2}$ does not change after 20 L dosing. The oxidized Ti $2p_{3/2}$ peak shifts 0.2 eV lower due to more oxidized Ti atoms with lower oxidation states such as $Ti_{2+}$. The BE of the metallic Nb $3d_{5/2}$ at 203.2 eV is 1.0 eV higher than the reported value [17] and cannot be explained by the presence of oxygen atoms on the surface and

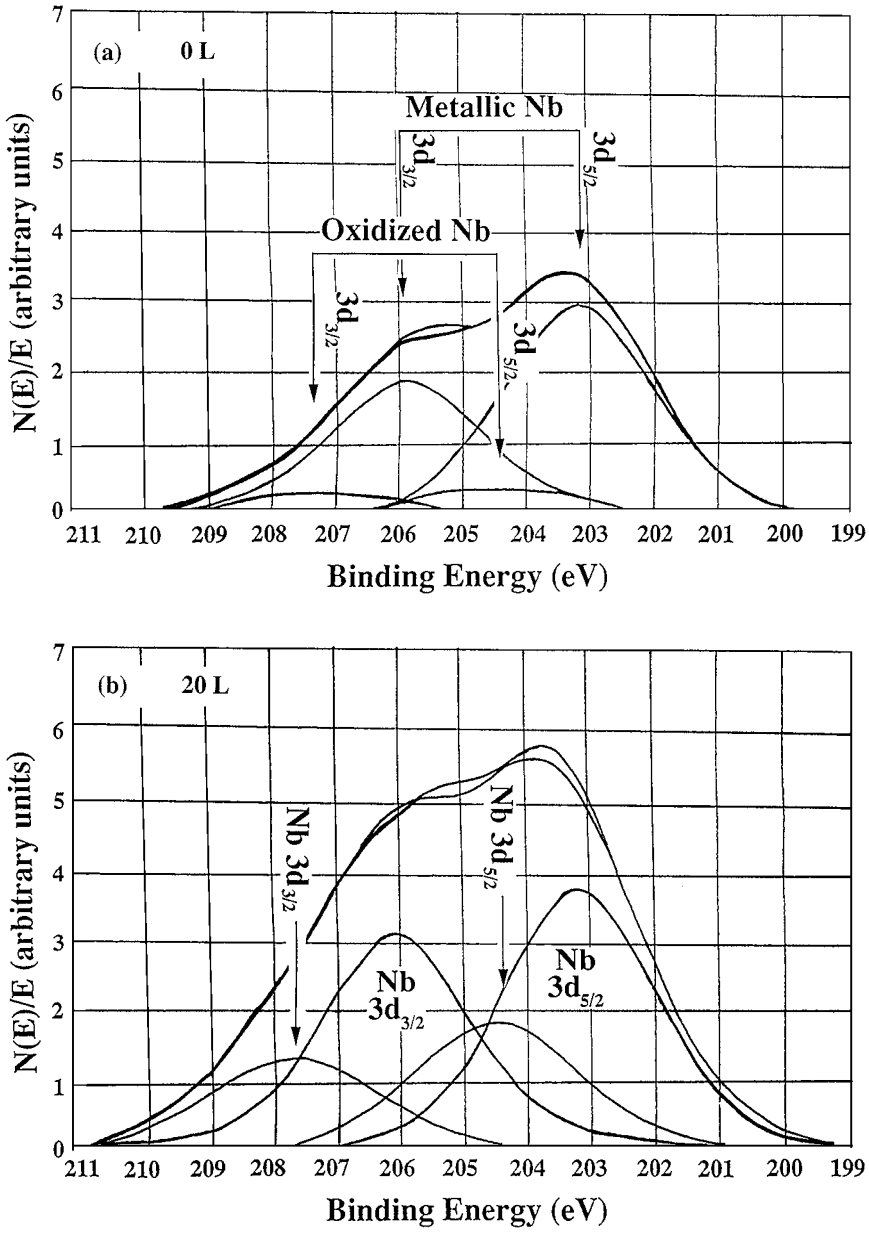


*Figure 5* The XPS spectra Nb 3d3/2 and 3d5/2 before oxygen dosing (a) and after 20 L oxygen dosing (b). Spectra were decomposed into oxidized state and metallic state by using a fitting program. It is clearly shown that the oxidized species of Al, Ti and Nb increased after oxygen dosing.

the surrounding atoms Al and Ti with lower electron negatives. However, the BE of the oxidized Nb $3d_{5/2}$ at 204.4 eV after sputtering approximates the reported value obtained for NbO [30], inferring that the Nb atoms attract electrons from Al and Ti atoms before dosing. After 20 L oxygen dosing, the metallic Nb $3d_{5/2}$ does not change which is similar to both metallic Al and metallic Ti cases. The oxidized Nb $3d_{5/2}$ peak shifts by 0.1 eV suggesting that less than one oxygen atom bonds to each Nb atom. In comparing the BE shifts before and after dosing, the BEs of all metallic species do not change, but oxidized species shift to lower BEs: oxidized Al decreased by 0.25 eV, oxidized Ti by 0.2 eV, and oxidized Nb by 0.1 eV. These shifts of the BEs for the oxidized species infer that oxygen bonds with Al and Ti form single, double and triple bonding.

After analyzing the spectra, the relative total concentrations of Al, Ti and Nb were obtained as a function of oxygen exposure (Fig. 6). The total Al content on the surface increases while both total Ti and total Nb contents decrease slightly with increasing oxygen exposure. The concentration profile suggests that the formation of the Al oxide layer dilutes Ti and Nb contents or Al diffuses towards the surface when the alloy is exposed to the oxygen, but the dilution seems more plausible. The initial oxidation of Ti aluminides in its formation of Al oxide would follow the process found for aluminum oxidation, which has been investigated with AES and XPS by Aranz and Palacio [33] and with XPS and high resolution electron energy loss spectroscopy (HREELS) by, Zhukov *et al*. [34] and Zhukov, Popova and Yates [35]. They reported the detection of three different Al 2p signals interpreted as the Al atoms forming one, two and three covalent O-Al bonds during Al oxidation.

The oxidation of the TiAlNb intermetallic of the present study involves the dissociative adsorption of oxygen similar to the gas-metal reactions of metals, as reviewed by Grabke and Horz [37] and more specifically to the initial oxidation of nickel by Holloway and

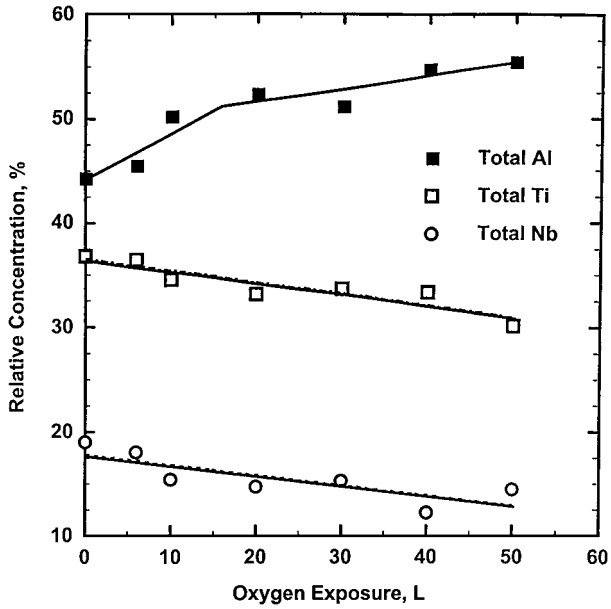


*Figure 6* The relative concentrations of total Al, total Ti and total Nb as function of oxygen exposure. The Al concentration increases with the increasing oxygen exposure but both Ti and Nb decrease.

Hudson [38] and Mitchell, Sewell and Cohen [39]. The adsorption of oxygen on Ti aluminide of the present study is proposed through the following reaction sequence incorporating the dissociative adsorption of oxygen and the single, double and triple bonding of oxygen with aluminum:

$$O_2 + 2V = 2O_{ad} \tag{1}$$

$$Al + O_{ad} \rightarrow AlO \tag{2}$$

$$AlO + O_{ad} \rightarrow AlO_2 \tag{3}$$

$$AlO_2 + O_{ad} \rightarrow AlO_3 \tag{4}$$

where $O_2$ initially dissociates upon adsorption onto two surface sites ($V$) and the adsorbed oxygen ($O_{ad}$) then reacts consecutively with Al, AlO, and $AlO_2$ to ultimately form $AlO_3$.

The corresponding reaction rates ($r_i$) are:

$$r_{O,ad} = k_1 p_{O_2} V^2 - k_1' C_{O,ad}^2 \tag{5}$$

$$-r_{Al} = k_2 a_{Al} C_{O,ad} \tag{6}$$

$$r_{AlO} = k_2 a_{Al} C_{O,ad} - k_3 C_{AlO} C_{O,ad} \tag{7}$$

$$r_{AlO_2} = k_3 C_{AlO} C_{O,ad} - k_4 C_{AlO_2} C_{O,ad} \tag{8}$$

$$r_{AlO_3} = k_4 C_{AlO_2} C_{O,ad} \tag{9}$$

where each $k_i$ is the forward rate constant, $k_i'$ is the backward rate constant, $p_{O_2}$ is the oxygen partial pressure, $C_i$ is the concentration of each species, and $a_{Al}$ is the activity of aluminum on the surface of the TiAlNb intermetallic.

With the rate determining step of oxygen adsorption Equation 1, the steady-state condition for the adsorbed oxygen and its consumption is:

$$r_{O,ad} = r_2 + r_3 + r_4 \tag{10}$$

where the adsorption rate of the oxygen onto surface, $r_{O,ad}$, is balanced by the consumption rate of oxygen, as given by the sum of reaction rates, $r_2$, $r_3$, and $r_4$, in Equations 2, 3, and 4, respectively, at the steady-state condition.

The consumption includes the series-parallel reactions for the single, double and triple binding of oxygen with aluminum and the rate equation results

$$k_1 p_{O_2} V^2 - k_1 C_{O,ad}^2 = k_2 C_{O,ad} a_{Al} + k_3 C_{O,ad} C_{AlO} + k_4 C_{O,ad} C_{AlO_2} \tag{11}$$

From Equation 11, an equation for $V$ can be derived.

$$V = \left[\left(k_1' C_{O,ad}^2 + k_2 C_{O,ad} a_{Al} + k_3 C_{O,ad} C_{AlO} + k_4 C_{O,ad} C_{AlO_2}\right) / k_1 p_{O_2}\right]^{1/2} \tag{12}$$

By substituting Equation 12 into the rate of formation of $O_{ad}$ Equation 5, the rate equation becomes

$$\frac{1}{S}\frac{dC_{O,ad}}{dt} = C_{O,ad}\alpha \tag{13}$$

where $S$ is the surface area and $\alpha = k_2 a_{Al} + k_3 C_{AlO} + k_4 C_{AlO_2}$.

After integration from the initial adsorbed oxygen ($C_{O,ad}^i$) to the final adsorbed oxygen ($C_{O,ad}^f$), the rate equation for adsorbed oxygen is

$$\ln\left[\frac{C_{O,ad}^f}{C_{O,ad}^i}\right] = S\alpha t \tag{14}$$

To determine the $AlO_3$ concentration with respect to the oxygen potential ($p_{O_2}$), the ratio of the rate of oxygen adsorption to the rate of $AlO_3$ formation was acquired as follows:

$$\frac{r_{O,ad}}{r_{AlO_3}} = \frac{\frac{2}{S}\frac{dp_{O_2}}{dt}}{\frac{1}{S}\frac{dC_{AlO_3}}{dt}} = \frac{k_2 C_{O,ad} a_{Al} + k_3 C_{O,ad} C_{AlO} + k_4 C_{O,ad} C_{AlO_2}}{k_4 C_{O,ad} C_{AlO_2}} \tag{15}$$

At steady state, $r_{AlO} = r_{AlO_2} = 0$ for reactions (2)–(3) which achieve equilibrium, and hence rate Equation 15 becomes

$$\frac{2dp_{O_2}}{dC_{AlO_3}} = \frac{k_2 C_{O,ad} a_{Al} + k_3 C_{O,ad}\left[\left[\frac{k_2 a_{Al}}{k_3}\right]\right] + k_4 C_{O,ad}\left[\left[\frac{k_2 a_{Al}}{k_4}\right]\right]}{k_4 C_{O,ad}\left[\left[\frac{k_2 a_{Al}}{k_4}\right]\right]} \tag{16}$$

$$\frac{dC_{AlO_3}}{dp_{O_2}} = \frac{2}{3} \tag{17}$$

By combining Equations 14 and 17, the $AlO_3$ concentration ($C_{AlO_3}$) with respect to Langmuir (i.e., $L = tp_{O_2}$)

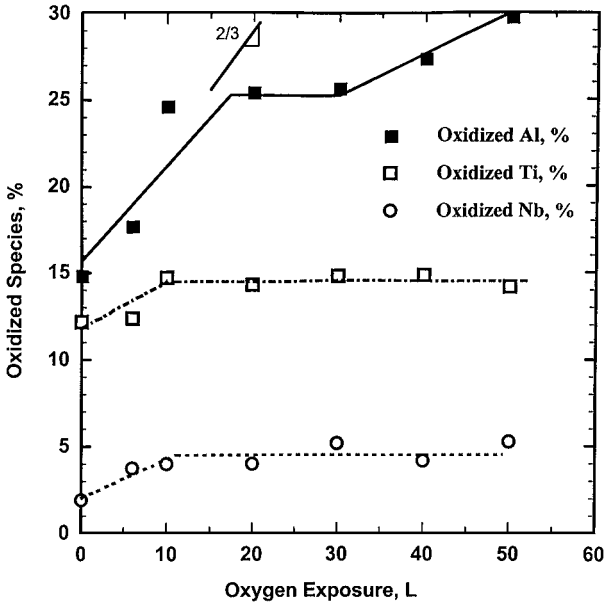


*Figure 7* The relative concentrations of oxidized Al, Ti, and Nb versus various oxygen exposures were plotted. A fast growth rate is observed at the beginning of the dosing and then the rate saturates. Al oxide grows again after 30 L oxygen dosing.

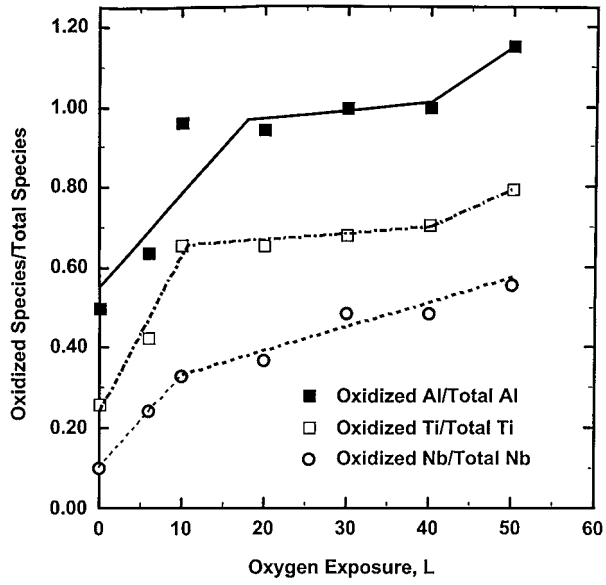


*Figure 8* Ratio of the concentration of oxidized state to the concentration of its own metallic state for Al, Ti, and Nb as function of oxygen exposure. It was observed when sample was exposed to more than 10 L oxygen that every oxidized Al atom associates to one metallic Al atom, 0.7 oxidized Ti atom corresponds to one metallic Ti atom, and the ratio for Nb is the smallest but steadily grows with the amount of oxygen on the surface.

is acquired as follows:

$$\frac{dC_{AlO_3}}{dL} = \frac{2}{3}\left[\frac{S\alpha}{\ln\left(C^f_{O,ad}/C^i_{O,ad}\right)}\right] \tag{18}$$

After decomposing the core-level XPS spectrum, the binding energy of each component was obtained for each oxidized species followed by their relative concentration, as shown in Fig. 7. The initial oxidation of each metal species (Al, Ti, and Nb) occurs within 10 L, which represents the juncture where the initial monolayer of $Al_2O_3$ reaches complete formation. For oxidized Al species, the slope in Fig. 7 approximates 2/3 indicating that oxygen adsorption or the activity of Al on the surface does not change significantly the slope of 2/3. In addition, if the AlO and $AlO_2$ species react quickly with adsorbed oxygen and cause a low AlO and $AlO_2$ content resulting in a negligible contribution, the $a_{AL}$ becomes a major parameter in the nominator. With the Taylor's series expansion of the logarithm of Equation 18, the equation approximates as follows:

$$\frac{dC_{AlO_3}}{dL} = \frac{2}{3}\left[\frac{S\left(k_2 a_{Al} + k_3 C_{AlO} + k_4 C_{AlO_2}\right)}{\ln\left(C^f_{O,ad}/C^i_{O,ad}\right)}\right] \cong \frac{2}{3}\left[\frac{S(k_2 a_{Al})}{1-\left(C^i_{O,ad}/C^f_{O,ad}\right)}\right] \tag{19}$$

For future studies with TiAl intermetallics having an increasing Al/Ti ratio, the $a_{Al}$ will also increase the rate of oxidation as expected. For Al/Ti ratios <0.5, the stability of $TiO_2$ becomes possible thermodynamically as noted by Rahmel and Spencer [12] at high temperatures and the authors of the present paper expect the thermodynamic stability of $TiO_2$ to apply at room temperature unless the kinetics cause a metastable oxide to form. It is clear that for the kinetics the formation for $TiO_2$ or a metastable titanium oxide on TiAl intermetallics at room temperature, the $Ti_{2p}$ peak must be examined to determine the variation of the Ti valency, similar to the study by Lu, Bernasek and Schwartz [33] on the oxidation of polycrystalline titanium surfaces. With Nb additions to the TiAl intermetallic, the $a_{AL}$ decreases and obviously cause a lowering of the oxidation rate indicated by the $dC_{AlO_3}/dL$ value.

For oxygen exposure greater than 30 L, the Al oxide content increases further as a result of either the formation of $Al_2O_3$ nuclei from the $AlO_3$ precursors or the initial rate (<10 L) results from the chemically adsorbed oxygen transforming to the oxide phase. The reaction model incorporating the adsorbed oxygen and the $AlO_3$ precursors agree with the results of Fig. 7, so the results suggest that initial oxidation occurs by oxygen adsorption, $AlO_3$ formation, followed by its transformation into oxide clusters or an $Al_2O_3$ layer. In fact, Arranz and Palacio [35] identified three stages of Al oxidation: first stage spanned the first 10 L, second stage extended from 10 L to approximately 1000 L, followed by the third stage at oxygen exposures >1000 L. The rate of transformation from $AlO_3$ precursors into the oxide clusters or layer is left for another study for oxygen exposures >50 L. Fig. 7 also shows that the highest oxidized species is Al oxide, then Ti oxide, and Nb oxide has the lowest concentration.

Since Al is the most populated species among the three metals on the surface before dosing, it seems that Al oxide should be the most abundant oxide, Ti oxide is the second and Nb is the least abundant oxide. Finally, the variation in the ratio of oxidized species to its own metallic species as function of oxygen exposure as shown in Fig. 8. Again, the ratio for Al is the highest. The fast growth rate is found at the beginning for all three of them and then the rate remains constant

at higher dosages (>10 L) for Al and Ti. Oxygen adsorption by Nb is the smallest but steadily grows with the amount of oxygen on the surface and Nb does not reach a plateau as acquired for Al and Ti.

## 4. Conclusions

a. From the XPS analysis, the $Al_2O_3$ forms and dilutes the Ti and Nb species as TiAlNb intermetallic oxidizes to form the initial monolayer.

b. The XPS spectra show a lowering of the binding energies of oxidized Al indicating the formation of AlO. The higher BE of oxidized Al results from $AlO_2$ and $AlO_3$ on the surface.

c. The binding energy shifts and the measured concentration of the oxidized species are consistent with a reaction sequence incorporating the dissociative adsorption of oxygen as a rate-determining step.

## References


1. W. SMARSLY and L. SINGHEISER, in "Materials for Advanced Power Engineering," Vol. 2, edited by D. Coutsouradis *et al*., (Kluwer Academic Publishers, Dordrecht, 1994) p. 1731.
2. K. MAKI, M. SHIODA, M. SAYASHI, T. SHIMIZU and S. ISOBE, *Materials Science and Engineering* **A153** (1992) 591.
3. D. EYLON, M. M. KELLER and P. E. JONES, *Intermetallics* **6** (1998) 703.
4. S. C. HUANG and J. C. CHESNUTT, in "Gamma TiAl and its Alloys," *Intermetallic Compounds*, Vol. 2, edited by J. H. Westbrook and R. L. Fleischer (John Wiley, New York, 1994) p. 73.
5. D. BANERJEE, in "$Ti_3Al$ and its Alloys," *Intermetallic Compounds*, Vol. 2, edited by J. H. Westbrook and R. L. Fleischer (John Wiley, New York, 1994) p. 91.
6. M. A. MORRIS, *Intermetallics* **4** (1996) 417.
7. F.-C. DARY and T. M. POLLOCK, *Materials Science and Engineering* **A208** (1996) 188.
8. J. D. H. PAUL, F. APPEL and R. WAGNER, *Acta Metallurgica* **46** (1998) 1075.
9. G. SAUTHOFF, *Intermetallics* **8** (2000) 1101.
10. S. K. VARMA, R. MAHAPATRA, C. HERNANDEZ, A. CHAN and E. CORRAL, *Material and Manufacturing Processes* **14** (1999) 821.
11. Y. SHIDA and H. ANADA, *Corrosion Science* **35** (1993) 945.
12. A. RAHMEL and P. J. SPENCER, *Oxidation of Metals* **35** (1991) 53.
13. S. BECKER, A. RAHMEL and M. SCHUTZE, *ibid*. **38** (1992) 425.
14. A. RAHMEL, W. J. QUADAKKERS and M. SCHUTZE, *Material and Corrosion* **46** (1995) 271.
15. T. K. ROY, R. BALASUBRAMANIAM and A. GHOSH, *Metallurgical and Materials Transactions* **27A** (1996) 3993.
16. S. TANIGUCHI and T. SHIBATA, *Intermetallics* **4** (1996) S85.
17. M. YOSHIHARA and K. MIURA, *ibid*. **3** (1995) 357.
18. K. MAKI, M. SHIODA, M. SAYASHI, T. SHIMIZU and S. ISOBE, *Materials Science and Engineering* **A153** (1992) 591.
19. A. HELLWIG, M. PALM and G. INDEN, *Intermetallics* **6** (1998) 79.
20. T. N. TAYLOR and M. T. PAFFETT, *Materials Science and Engineering* **A153** (1992) 584.
21. M. R. SHANABARGER, *ibid*. **A153** (1992) 608.
22. *Idem*., *Applied Surface Science* **134** (1998) 179.
23. R. W. BEYE and R. GRONSKY, *Acta Metall. Mater*. **42** (1994) 1373.
24. R. BEYE, M. VERWERFT, J. T. M. DE HOSSON and R. GRONSKY, *Acta Mater*. **44** (1996) 4225.
25. J. GENG, G. GANTNER, P. OELHAFEN and P. K. DATTA, *Applied Surface Science* **158** (2000) 64.
26. S. ZADOR and C. B. ALCOCK, *High Temperature Science* **16** (1983) 187.
27. Scientific Group Thermodata Europe (SGTE) GTT Technologies, Herzogenrath, Germany.
28. P. KOFSTAD, "Nonstoichiometry, Diffusion and Electrical Conductivity in Binary Metal Oxides" (Krieger Publishing Company, Malabar, Florida, 1983) p. 139.
29. P. W. WANG, S. BATER, L. P. ZHANG, M. ASCHERL and J. H. CRAIG, JR., *Applied Surf. Sci*. **90** (1995) 413.
30. Wagner, Riggs, Davis, Moulder and Muilenburg, Handbook of X-ray Photoelectron Spectroscopy, Perkin-Elmer Corp. Eden Prairie, MN, 1979.
31. P. W. WANG, S. SUI and W. DURRER, *Appl. Surf. Sci*. **178** (2001) 98.
32. P. W. WANG, Y. QI and D. O. HENDERSON, *J. Non-Crystalline Solids* **224** (1998) 31.
33. A. ARRANZ and C. PALACIO, *Surface Science* **355** (1996) 203.
34. V. ZHUKOV, I. POPOVA, V. FOMENKO and J. T. YATES, *ibid*. **441** (1999) 240.
35. V. ZHUKOV, I. POPOVA and J. T. YATES, *Surface Science* **441** (1999) 251.
36. G. LU, S. L. BERNASEK and J. SCHWARTZ, *Surface Science* **458** (2000) 80.
37. H. J. GRABKE and G. HORZ, *Annual Reviews of Material Science* **7** (1977) 155.
38. P. H. HOLLOWAY and J. B. HUDSON, *Surface Science* **43** (1974) 123.
39. D. F. MITCHELL, P. B. SEWELL and M. COHEN, *ibid*. **69** (1977) 310.



*Received 25 February*
*and accepted 24 September 2002*